Nuclear Physics B285 [FS19] (1987) 391–409
North-Holland, Amsterdam

NONCANONICAL PATH AND SURFACE SIMULATION

Bernd BAUMANN*

II. Institut für Theoretische Physik der Universität Hamburg, Luruper Chaussee 149, D-2000 Hamburg 50, FR Germany

Received 29 October 1986
(Revised 8 January 1987)

A Monte Carlo process for the simulation of random walks and random surfaces is proposed. It is based on the canonical algorithm of Berg, Billoire and Förster, but uses a length (area) dependent coupling constant. The method is applied to determine the critical coupling constant of the planar random surface model without spikes in various dimensions. Also the mean-field behaviour of this model is derived and β_0^{MF} is compared to the data. It is shown, that the string tension of the model for $d \to \infty$ is dominated by the minimal surface spanned by the Wilson loop.

1. Introduction

During the last years much effort has been put into understanding lattice random walk and surface systems. Despite their complexity many properties have been derived with analytical methods [1, 2, 11, 14, 16, 17], some of which we review in the following sections. Nevertheless, as has been pointed out by Fröhlich [3], it seems that in order to make further progress the use of numerical methods is unavoidable. In 1981 Berg and Förster suggested a Monte Carlo procedure for the simulation of random walks [4]. The method has the advantage of being very flexible. It can be used for the investigation of free random walks, random walks without spikes, self-avoiding random walks and more general systems [5]. A shortcoming of the method is that it has an autocorrelation time of order $\langle L \rangle^{2+2\nu}$, where L is the length of the path and ν is the inverse of the Hausdorff dimension. Beretti and Sokal suggested a Monte Carlo process for random walks which has an autocorrelation time of order $\langle L \rangle^2$ [8]. This procedure has been used by de Forcrand, Koukiou and Petritis to simulate the self-avoiding walk on an hexagonal lattice [9]. One of their conclusions is that the method is not suitable for the simulation of walks with both end-points fixed. So in this case we have to adhere to the procedure of Berg and Förster. The latter method has a direct generalization to the case of random surfaces. It is extremely important to have a tool for the investigation of self-avoid-

* Supported by Deutsche Forschungsgemeinschaft.

ing surfaces, surface models which take the curvature of the surfaces into account (see ref. [15]) and other systems. Unfortunately the computer code for surfaces becomes very complicated [6, 7]. In this paper we make a proposal how to modify the procedure in order to increase its efficiency. The method is used to perform a high precision calculation of the critical coupling constant for the planar random surface model without spikes in various dimensions. Furthermore we compare the results with the corresponding mean-field values.

2. The models

For the reader's convenience we give a short summary of the definition of the models which have been investigated in the past. In the case of the random walks the 2-point-function is defined through

$$G_\beta(x, y) = \sum_{\omega:\, x \to y} \mathrm{e}^{-\beta L(\omega)}$$

$$= \sum_{L = L_{\min}}^{\infty} n(L)\mathrm{e}^{-\beta L}. \tag{2.1}$$

ω is a path on the lattice connecting the points x and y and $L(\omega)$ its length. The models considered here are distinguished according to the properties of the walks which contribute to the sum in (2.1).

Prominent examples are:

(i) The bosonic random paths (BRP). All walks contribute.

(ii) The fermionic random paths (FRP). All walks without spikes contribute. A spike is formed by two consecutive steps of the walk which occupy the same lattice link.

(iii) The self-avoiding random paths (SARP). All those walks contribute which meet each lattice site at most once.

The path entropy is generally assumed to behave like

$$n(L) \sim L^{\varepsilon}\mathrm{e}^{\beta_0 L}, \qquad L \to \infty, \tag{2.2}$$

where β_0 is the critical coupling constant and ε is a critical exponent. In the case of the closed bosonic and fermionic random walks in 4 dimensions there exist the following useful expressions for the entropy [12]:

$$n_{\mathrm{BRP}}(L) = \sum_{l=0}^{L/2} \binom{2l}{l}^2 \binom{L-2l}{\frac{1}{2}L-l}^2 \binom{L}{2l} \tag{2.3}$$

and

$$n_{\mathrm{FRP}}(L) = n_{\mathrm{BRP}}(L) + 6 - 8\delta_{L,0} - 7\delta_{L,2} + \sum_{l=1}^{L/2} (-1)^l 7^l \left[\binom{L-l}{l} + \binom{L-l-1}{l-1} \right] n_{\mathrm{BRP}}(L-2l), \quad (2.4)$$

where L is even. We used these formulae to calculate the entropy with infinite precision up to $L = 100$. The notable result is that the entropy at $L = 100$ deviates from the asymptotic expression by roughly 2.5%. So we find it necessary to simulate the models at lengths (areas) larger than 100 in order to obtain reliable estimates for the quantities β_0 and ε.

For each of the above presented path models there exists a natural analogue for surfaces:

(i) The planar random surface model (PRS). All orientable surfaces with planar topology contribute.

(ii) The planar random surface model without spikes (PRSWS). Like the PRS, with the additional constraint that surfaces which contain spikes do not contribute. A spike consists out of two connected monomers which occupy the same plaquette.

(iii) The self-avoiding random surface model (SARS). Those planar and orientable surfaces contribute, which occupy each lattice link at most once.

Instead of (2.1) we have now

$$G_\beta(\gamma_1, \ldots, \gamma_n) = \sum_{S \in \mathcal{S}(\gamma_1, \ldots, \gamma_n)} e^{-\beta |S|}, \quad (2.5)$$

where S is a surface which has the loops γ_i as its boundary. $|S|$ denotes the area of S. The entropy is assumed to behave like (2.2), where one has to replace the length by the area.

Let us compile the most important features of the PRS and PRSWS (for the definitions needed we refer to ref. [1, 2]):

For the PRS it has been shown [2] that the mean-field values of the critical indices describe the properties of the model in all dimensions $\geqslant 2$. In particular this means that the Hausdorff dimension d_{H} is 4 and η, the anomalous dimension of the 2-loop function, is zero. The continuum limit of the string tension is infinite. In contrast to a universality conjecture it has been shown in [10], that the PRSWS in 4 dimensions has a nonvanishing anomalous dimension of the 2-loop-function. The Hausdorff dimension comes out to be 4. The PRSWS is the simplest known lattice surface model showing nontrivial critical behaviour. In this article we demonstrate that the model possesses universal mean-field behaviour in high dimensions.

Remark. In the somewhat pathological case of 2 dimensions the PRS and PRSWS show completely different behaviour. Here a local constraint (no spikes

allowed!) makes the PRSWS (almost) identical to SARS. The Hausdorff dimension becomes equal to the canonical dimension of surfaces, that is $d_H = 2$. The string tension is equal to β and the mass gap is infinite. We see that in 2 dimensions PRSWS and lattice gauge theories are trivial in a very similar way.

Recently Polyakov has proposed to consider a string theory with an action that takes the extrinsic curvature of the surfaces into account [18]. A lattice surface model with this property has been introduced by Durhuus and Jonsson [17]. They point out, that the PRSWS corresponds to a certain limit of their model. This yields a more physical interpretation of the "no spike constraint", which originally has been incorporated in analogy to the fermionic random walks.

3. The Monte Carlo procedure of Berg, Billoire and Förster

We start by summarizing the Monte Carlo procedure for random surfaces as introduced by Berg, Billoire and Förster [4, 7]. We restrict the discussion to surfaces, since the treatment of walks is simpler and follows the same line.

Suppose one is given a surface on the lattice belonging to a certain class (planar, self-avoiding, ...). The MC process consists of performing a sequence of local deformations according to some rules. The deformations have to be such, that the surfaces obtained from a parent surface belong to the same specified class. We call the 2-cells which constitute the surface monomers to distinguish them from the plaquettes of the lattice. The deformations are realized via shifts of monomers. Such shifts are specified by the following rules:

(i) Make a cut which isolates a monomer p from the surface. Call p the shift monomer.

(ii) The shift monomer defines a plane. Shift the monomer into a direction perpendicular to this plane. Clearly, the boundary of the shift monomer sweeps out four plaquettes p_i, $i = 1, 2, 3, 4$.

(iii) (a) If p_i is not occupied by a neighbour of p, place a monomer there.

(b) If the plaquette p_i is occupied with a neighbour of p, remove the neighbour monomer.

(iv) After this procedure has been performed on all plaquettes p_i, the pieces are glued together along their boundaries.

An example of a shift is depicted in fig. 1. In this way only changes of area of 0, ± 2 and ± 4 are possible.

Now we go from one surface to the next by the following steps:

(a) Choose randomly one of the monomers building up the surface. It is taken to be the shift monomer.

(b) Then choose randomly one of the directions perpendicular to the shift monomer.

(c) Check if an imposed constraint, for example self-avoidingness, would be violated if the chosen monomer is shifted into this direction.

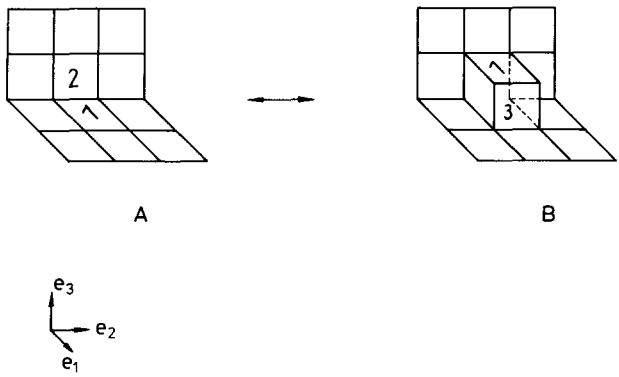

Fig. 1. Example of a shift. When, starting from A, monomer 1 is shifted into the direction e_3, configuration B is the result. During the shift monomer 2 is deleted and monomer 3 as well as those monomers lying in the plane spanned by e_1 and e_3 are created. The same configuration would result from a shift of 2 into direction e_1.

(d) If no constraint is violated calculate Δ, the amount of change in surface area, for the proposed shift.

(e) Perform the shift with a probability $p(\Delta)$ that depends on the change in area.

Thus we obtain for the shift probability:

$$W(\mathrm{S} \to \mathrm{S}') \sim \frac{1}{|\mathrm{S}|} p(\Delta) \chi(\mathrm{S}'). \tag{3.1}$$

Here $\chi(\mathrm{S}')$ is 0 or 1, depending on whether a constraint is violated or not. $\chi(\mathrm{S}')$ is also set to zero if a proposed shift has no inverse and in some other cases [7]. We demand that the following conditions are fulfilled:

(i) Normalization

$$\sum_{\mathrm{S}'} W(\mathrm{S} \to \mathrm{S}') = 1,$$

(ii) Ergodicity.

(iii) Detailed balance (DB)

$$P(\mathrm{S}) W(\mathrm{S} \to \mathrm{S}') = W(\mathrm{S}' \to \mathrm{S}) P(\mathrm{S}'). \tag{3.2}$$

From DB and (3.1) one can read off that we obtain the probability distribution

$$P(\mathrm{S}) \sim |\mathrm{S}| \mathrm{e}^{-\beta |\mathrm{S}|}, \tag{3.3}$$

instead of a pure Boltzmann distribution. Detailed balance implies

$$p(\Delta)/p(-\Delta) = \mathrm{e}^{-\Delta\beta}. \tag{3.4}$$

The normalization condition for the unconstrained system can be written as

$$\pi(\mathrm{S},\mathrm{p}) = \pi_{\mathrm{A}\cdot\mathrm{B}} = 1 - \sum_{e_\perp} p(\Delta), \tag{3.5}$$

where $\pi(\mathrm{S},\mathrm{p})$ is the probability that no shift takes place after the shift monomer p has been chosen and $e_\perp$ is the shift direction. In the notation of [7], A labels different types of surface geometry and B labels different types of shifts.

Working out (3.5) for all cases gives

$$\begin{aligned}
\pi_{1\cdot1} &= 1 - (2d-4)\,p(+4),\\
\pi_{2\cdot1} &= 1 - p(+2) - (2d-5)\,p(+4),\\
\pi_{3\cdot1} &= 1 - 2p(+2) - (2d-6)\,p(+4),\\
\pi_{3\cdot2} &= 1 - p(0) - (2d-5)\,p(+4),\\
\pi_{4\cdot1} &= 1 - 3p(+2) - (2d-7)\,p(+4),\\
\pi_{4\cdot2} &= 1 - p(0) - p(+2) - (2d-6)\,p(+4),\\
\pi_{4\cdot3} &= 1 - p(-2) - (2d-5)\,p(+4),\\
\pi_{5\cdot1} &= 1 - 4p(+2) - (2d-8)\,p(+4),\\
\pi_{5\cdot2} &= 1 - p(0) - 2p(+2) - (2d-7)\,p(+4),\\
\pi_{5\cdot3} &= 1 - 2p(0) - (2d-6)\,p(+4),\\
\pi_{5\cdot4} &= 1 - p(-2) - p(+2) - (2d-6)\,p(+4),\\
\pi_{5\cdot5} &= 1 - p(-4) - (2d-5)\,p(+4).
\end{aligned} \tag{3.6}$$

Detailed balance (3.4) yields two equations for the five unknown $p(\Delta)$. The remaining freedom can be used to make three of the null-shift probabilities vanish. The choice

$$\pi_{5\cdot3} = \pi_{5\cdot4} = \pi_{5\cdot5} = 0 \tag{3.7}$$

optimizes the algorithm and is consistent in the sense that all probabilities lie in the

range between zero and one. This leads to

$$p(-4) = \frac{1}{1+(2d-5)\kappa^2},$$

$$p(-2) = \frac{1+\kappa^2}{(1+\kappa)} p(-4),$$

$$p(0) = \tfrac{1}{2}(1+\kappa^2)\, p(-4),$$

$$p(+2) = \kappa p(-2),$$

$$p(+4) = \kappa^2 p(-4), \tag{3.8}$$

with $\kappa = \mathrm{e}^{-2\beta}$. More details and some subtle points can be found in ref. [7].

4. The noncanonical weight factor

In our previous work we found it mandatory to use a microcanonical ensemble for both path and surface simulation [10]. We obtained an approximation to a microcanonical ensemble by choosing $\beta < \beta_0$ and introducing an upper bound on the area. This method has the appealing feature that it can be realized very easily. However it also has its problems. Surfaces with an area smaller than the upper bound are exponentially suppressed. At the upper bound it does not make sense to collect data, because there the ergodicity condition is not fulfilled in some of the models. Also a fixed bound might decrease the flexibility of the lattice surface, which could slow down the motion through the space of surfaces. (In fact, this has been the reason for our decision not to introduce a lower bound on the area). Another possible implementation of the microcanonical ensemble consists in making the shift probabilities area dependent. In general however this leads to severe technical problems, in particular if one wants to simulate large surfaces. These problems can be avoided by the use of the following probability distribution

$$P(\mathrm{S}) \sim c\big(\beta_{|\mathrm{S}|}\big)|\mathrm{S}|\mathrm{e}^{-\beta_{|\mathrm{S}|}|\mathrm{S}|}, \tag{4.1}$$

with

$$\beta_{|\mathrm{S}|} = \begin{cases} \beta_l < \beta_0, & \text{if } |\mathrm{S}| < A_1, \\ \beta_u > \beta_0, & \text{if } |\mathrm{S}| \geqslant A_1, \end{cases} \tag{4.2}$$

for some fixed A_1. Indeed, this leads to area-dependent shift probabilities: $p(\Delta) \to p_{|\mathrm{S}|}(\Delta)$ and $\pi_{\mathrm{A}\cdot\mathrm{B}} \to \pi^{|\mathrm{S}|}_{\mathrm{A}\cdot\mathrm{B}}$. Since $|\Delta| \leqslant 4$ we have to distinguish only six different situations: $|\mathrm{S}| < A_1 - 4$, $|\mathrm{S}| = A_1 - 4$, $|\mathrm{S}| = A_1 - 2$, $|\mathrm{S}| = A_1$, $|\mathrm{S}| = A_1 + 2$ and $|\mathrm{S}|$

$> A_1 + 2$. The DB condition reads now

$$\frac{c(\beta_{|S|})}{c(\beta_{|S|+\Delta})} e^{\Delta\beta_{|S|+\Delta}} e^{|S|(\beta_{|S|+\Delta}-\beta_{|S|})} = \frac{p_{|S|+\Delta}(-\Delta)}{p_{|S|}(+\Delta)} . \tag{4.3}$$

To simplify the formulae we introduce some notation:

$$\omega := \frac{c(\beta_u)}{c(\beta_l)} , \qquad \mathscr{E} := e^{-A_1(\beta_u-\beta_l)} ,$$

$$p_{|S|}(\Delta) = \begin{cases} p_{\kappa_l}(\Delta), & \text{for } |S| < A_1 - 4 \\ p_{-4}(\Delta), & \text{for } |S| = A_1 - 4 \\ \vdots & \vdots \\ p_{+2}(\Delta), & \text{for } |S| = A_1 + 2 \\ p_{\kappa_u}(\Delta), & \text{for } |S| > A_1 + 2 . \end{cases} \tag{4.4}$$

The probabilities $p_{\kappa_i}(\Delta)$ are chosen to be identical to the probabilities $p(\Delta)$ in (3.8) with κ being equal to $\kappa_i = e^{-2\beta_i}$, $i = l, u$ respectively. Detailed balance implies:

$$\begin{aligned} p_{-4}(-4) &= p_{\kappa_l}(-4) , \\ p_{-4}(-2) &= p_{\kappa_l}(-2) , \\ p_{-4}(+2) &= \kappa_l p_{-2}(-2) , \\ p_{-4}(+4) &= \omega\kappa_l^2 \mathscr{E} p_0(-4) , \\ p_{-2}(-4) &= p_{\kappa_l}(-4) , \\ p_{-2}(+2) &= \omega\kappa_l \mathscr{E} p_0(-2) , \\ p_{-2}(+4) &= \omega\kappa_l\kappa_u \mathscr{E} p_{+2}(-4) , \\ p_0(+2) &= \kappa_u p_{+2}(-2) , \\ p_0(+4) &= p_{\kappa_u}(+4) , \\ p_{+2}(+2) &= p_{\kappa_u}(+2) , \\ p_{+2}(+4) &= p_{\kappa_u}(+4) . \end{aligned} \tag{4.5}$$

The remaining detailed balance conditions are not affected. This means that (3.4) is obeyed for the cases not listed in (4.5) with β being equal to β_l or β_u respectively. The null-shift probabilities are also area dependent. We define: $\pi^{\Delta}_{A\cdot B} := \pi^{A_1+\Delta}_{A\cdot B}$. Demanding:

$$\begin{aligned} \pi^{\Delta}_{5\cdot 3} &= 0 \qquad \text{for } \Delta \in \{-4,-2,0,+2\}, \\ \pi^{\Delta}_{5\cdot 4} &= 0 \qquad \text{for } \Delta \in \{-2,0,+2\} \\ \pi^{\Delta}_{5\cdot 5} &= 0 \qquad \text{for } \Delta \in \{-2,0\}, \end{aligned} \tag{4.6}$$

and

$$\mathscr{E} = \frac{1}{\omega} \tag{4.7}$$

determines all probabilities in a consistent way and makes the probability distribution continuous at A_1. However it is more efficient to have as many transistion probabilities as possible unmodified in comparison with the old algorithm, allowing for a discontinuous distribution at $|S| = A_1$. The optimal choice is

$$\begin{aligned} &\pi^{\Delta}_{5\cdot 3} = \pi^{\Delta}_{5\cdot 4} = \pi^{\Delta}_{5\cdot 5} = 0 \qquad \text{for } \Delta \in \{-4,0,+2\}, \\ &\pi^{-2}_{5\cdot 3} = 0, \end{aligned} \tag{4.8}$$

and

$$\mathscr{E} = \frac{p_{\kappa_l}(-4)}{\omega p_{\kappa_u}(-4)}. \tag{4.9}$$

It corresponds to

$$\begin{aligned} p_{-4}(\Delta) &= p_{\kappa_l}(\Delta), \\ p_{-2}(-4) &= p_{\kappa_l}(-4), \\ p_{-2}(-2) &= p_{\kappa_l}(-2), \\ p_{-2}(0) &= \tfrac{1}{2} - (d-3)p_{\kappa_l}(-4), \\ p_{-2}(+2) &= \frac{p_{\kappa_l}(+4)p_{\kappa_u}(-2)}{\kappa_l p_{\kappa_u}(-4)}, \\ p_{-2}(+4) &= \frac{\kappa_u p_{\kappa_l}(+4)}{\kappa_l}, \\ p_0(\Delta) &= p_{\kappa_u}(\Delta), \\ p_{+2}(\Delta) &= p_{\kappa_u}(\Delta). \end{aligned} \tag{4.10}$$

This choice is consistent in the sense that all resulting probabilities are between zero and one.

Sometimes one needs to generate surfaces in a range $|S| \in [A_{\min}, A_{\max}]$ with equal frequencies. This can easily be achieved by using the above described distribution (4.1) with

$$\beta_{|S|} = \begin{cases} \beta_l < \beta_0, & \text{if } |S| < A_{\min}, \\ \beta_m \approx \beta_0, & \text{if } A_{\min} \leqslant |S| < A_{\max}, \\ \beta_u > \beta_0, & \text{if } |S| \geqslant A_{\max}. \end{cases} \tag{4.11}$$

5. The noncanonical weight factor at work

Let us perform MC simulations with the weight factor (4.1), (4.2). The relative frequency for the generation of surfaces with $|S| = A$, $A \gg 1$, is

$$\bar{N}(A) \sim c(\beta_A) A^{\varepsilon+1} \mathrm{e}^{-(\beta_A - \beta_0)A}. \tag{5.1}$$

Therefore it follows for $A < A_1$ and $A' > A_1$, that

$$\bar{N}(A') = \omega \left(\frac{A'}{A}\right)^{\varepsilon+1} \exp((\beta_l - \beta_0)A - (\beta_u - \beta_0)A')\bar{N}(A). \tag{5.2}$$

The relative frequency is asymmetrically distributed around A_1. This is due to the following reasons:

(i) We have a discontinuity in $P(S)$ at $|S| = A_1$ by construction.

(ii) The factor $A^{\varepsilon+1}$.

(iii) Finite size effects.

(iv) Finally we have to use a guess for β_0 as input which, via (4.2), contributes to the asymmetry.

Our aim is to take advantage from (iv) and to use the asymmetry to determine β_0. With $A = A_1 - \alpha_1$ and $A' = A_1 + \alpha_2$ we obtain from (5.2) an estimator of β_0:

$$\bar{\beta}_0 = \frac{1}{\alpha_1 + \alpha_2} \left\{ \beta_l \alpha_1 + \beta_u \alpha_2 + \log \frac{p_{\kappa_u}(-4)\bar{N}(A_1 + \alpha_2)}{p_{\kappa_l}(-4)\bar{N}(A_1 - \alpha_1)} - (\varepsilon + 1) \log \frac{A_1 + \alpha_2}{A_1 - \alpha_1} \right\}. \tag{5.3}$$

Usually one has some a priori bounds on ε. For PRSWS we assume $-1 \leqslant \varepsilon + 1 \leqslant 0$. Choosing $A_1 \approx 5000$ and $\alpha_i \ll A_1$ the contribution of the last term in (5.3) is small ($\leqslant 2 \times 10^{-4}$).

TABLE 1
Statistics from simulation of PRSWS

d	A_1	β_l	β_u	Total number of iterations	Iterations for thermalisation
3	4999	0.525	1.525	42×10^7	2×10^7
4	"	0.690	1.690	17×10^7	1×10^7
6	"	0.900	1.900	17×10^7	1×10^7
8	"	1.005	2.005	17×10^7	1×10^7
8	9499	1.005	2.005	17×10^7	1×10^7
10	4999	1.075	2.075	34×10^7	2×10^7
12	"	1.150	2.150	50×10^7	2×10^7
26	"	1.410	2.410	50×10^7	2×10^7

We performed simulations of PRSWS in various dimensions. The statistics we have collected are summarized in table 1. About 100 hours of CPU time have been used on the Siemens-Fujitsu 7.882 computer of Hamburg University. The program is written in Fortran 77 and was run with optimization level 3, which is slightly faster than level 2 ($\approx 10\%$).

Results can be found in table 2. Error bars for the generation frequency $\bar{N}(A)$ have been estimated in the standard way. That is, first we divide the sequence of data into bins of different size; then for all these divisions error bars are calculated, assuming the bin-means are independent events. The values obtained in this way, which are in some range approximately independent of the bin size, are taken as error bars of $\bar{N}(A)$. The maximum number of bins consistent with this error bar can also be found in table 2. Unfortunately in three dimensions no such constant error bar can be found. Here we take the value calculated from a five bin division of the data.

Next we calculate $\bar{\beta}_0$ by using the numbers from table 2 and setting $\alpha_1 = \alpha_2 := \alpha = 2, 4$. Error bars for $\bar{\beta}_0$ are calculated using the standard formula for the propagation of errors. We draw the bin values of the data pairs into the $\bar{N}(A_1 - 2)$ versus $\bar{N}(A_1 + 2)$ plane. These plots reveal, that anticorrelations of the two frequencies have to be taken into account, when one calculates the errors. The values we obtained for $\bar{\beta}_0$ from $\alpha = 2$ and $\alpha = 4$ are consistent with each other. The same is true for the corresponding error bars. In eight dimensions we performed simulations at $A_1 = 4999$ and at $A_1 = 9449$. The results for $\bar{\beta}_0$ from large and very large surfaces are consistent within error bars. We conclude, that finite-size effects are small. Next we calculated $\bar{\beta}_0$ for individual bins. The meanvalue $\hat{\beta}_0$ of these quantities as well as the corresponding error is in good agreement with $\bar{\beta}_0$ and $\Delta\bar{\beta}_0$ for all d. Therefore the distribution of the $\bar{\beta}_0$ is assumed to be weakly biased. In ref. [10] we presented estimates for β_0 in four and eight dimensions. The values obtained from the noncanonical method lie in the ranges given there.

All results concerning β_0 are summarized in table 3.

TABLE 2
Results of simulation of PRSWS in various dimensions

	$d = 3$	Number of bins = 5
A	$\bar{N}(A)$	$\Delta\bar{N}(A)$
4995	0.13383	0.00047
4997	0.23274	0.00029
4999	0.33545	0.00214
5001	0.07902	0.00091
5003	0.01798	0.00030
	$d = 4$	Number of bins = 16
A	$\bar{N}(A)$	$\Delta\bar{N}(A)$
4995	0.07079	0.00013
4997	0.19213	0.00029
4999	0.43992	0.00016
5001	0.16182	0.00027
5003	0.05941	0.00020
	$d = 6$	Number of bins = 16
A	$\bar{N}(A)$	$\Delta\bar{N}(A)$
4995	0.07366	0.00015
4997	0.19604	0.00022
4999	0.43905	0.00019
5001	0.15811	0.00021
5003	0.05676	0.00016
	$d = 8$	Number of bins = 8
A	$\bar{N}(A)$	$\Delta\bar{N}(A)$
4995	0.07114	0.00017
4997	0.19307	0.00021
4999	0.43921	0.00018
5001	0.16130	0.00022
5003	0.05926	0.00013
	$d = 8$	Number of bins = 8
A	$\bar{N}(A)$	$\Delta\bar{N}(A)$
9495	0.07111	0.00022
9497	0.19322	0.00027
9499	0.43956	0.00023
9501	0.16114	0.00031
9503	0.05912	0.00015

TABLE 2 (Continued)

$d = 10$	Number of bins = 8	
A	$\bar{N}(A)$	$\Delta\bar{N}(A)$
4995	0.06768	0.00012
4997	0.18884	0.00015
4999	0.43924	0.00011
5001	0.16592	0.00022
5003	0.06267	0.00010
$d = 12$	Number of bins = 24	
A	$\bar{N}(A)$	$\Delta\bar{N}(A)$
4995	0.06968	0.00009
4997	0.19096	0.00015
4999	0.44026	0.00010
5001	0.16310	0.00013
5003	0.06041	0.00009
$d = 26$	Number of bins = 24	
A	$\bar{N}(A)$	$\Delta\bar{N}(A)$
4995	0.06681	0.00009
4997	0.18566	0.00017
4999	0.44290	0.00013
5001	0.16669	0.00017
5003	0.06256	0.00012

TABLE 3
Results concerning β_0

d	α	Number of bins	$\bar{\beta}_0$	$\Delta\bar{\beta}_0$	$\hat{\beta}_0$	$\Delta\hat{\beta}_0$	From ref. [10]
3	2	5	0.7833	0.0026	0.7832	0.0026	
	4	5	0.7883	0.0025			
4	2	16	1.1898	0.0007	1.1898	0.0007	$1.180 < \beta_0 < 1.195$
	4	16	1.1896	0.0006			
6	2	16	1.3891	0.0006	1.3891	0.0006	
	4	16	1.3889	0.0006			
8	2	8	1.5042	0.0006	1.5042	0.0006	$1.502 < \beta_0 < 1.507$
	4	16	1.5042	0.0006			
8	2	8	1.5038	0.0008	1.5038	0.0008	
	4	8	1.5040	0.0007			
10	2	8	1.5880	0.0005	1.5880	0.0005	
	4	8	1.5881	0.0004			
12	2	24	1.6534	0.0004	1.6534	0.0004	
	4	24	1.6536	0.0003			
26	2	24	1.9209	0.0004	1.9209	0.0004	
	4	24	1.9207	0.0004			

Finally let us comment on the case $d = 3$. In three dimensions the Monte Carlo process for PRSWS is not ergodic. A certain class of surfaces cannot be generated with the described shift procedure, as has been described in ref. [7]. Therefore the value of $\bar{\beta}_0$ for $d = 3$, given in table 3, is not the critical coupling constant of the PRSWS, but of a model which is built from a subset of the surfaces constituting the PRSWS.

6. Mean-field analysis of the PRSWS

In 1979 Drouffe, Parisi and Sourlas presented a mean-field approximation for the study of lattice gauge theories [13]. Their method can be used for the investigation of random surface systems in high dimensions [2, 3]. In this section we present the mean-field analysis of PRSWS.

The starting point is the observation, that in high dimensions the loop correlation functions are dominated by so called "tree-like surfaces". In order to see what the essential features of tree-like surfaces are, we demonstrate how they can be constructed in the various models. We restrict ourselves to surfaces with one minimal boundary loop.

PRS. Take two monomers and place them on top of each other. Let us call such an object a "tree element". Choose one of its eight links. Now we have two possibilities to proceed:

(a) The chosen link and the one sharing its position are identified. This means, that the monomers constituting the tree element become connected.

(b) Place a new tree element onto the lattice in such a way that one of its links can be identified with the link under consideration.

Repeat this procedure until a surface with the appropriate boundary has been created. The set of surfaces which can be built up in this way form the tree surfaces of the PRS.

SARS. Here the tree elements are complexes formed by the edges of a cube. For the loops of length four we again have a choice:

(a) Put a monomer onto the loop and identify its boundary with the links of the loop.

(b) Place a new tree element onto the lattice and identify one of its loops with the loop under consideration.

Iterate this procedure until a surface has been created which has a four-link loop γ as boundary. The set of self-avoiding surfaces which can be built in this way forms the tree surfaces of SARS. We see that tree surfaces are the "thinnest" possible surfaces in the considered model.

What are the tree surfaces in PRSWS? At a first sight it may be tempting to think of cubes, cut along their edges, as the tree elements. However there is also the

possibility to have doubly occupied plaquettes if to all of its four boundaries other allowed configurations are attached. Of course then, if we want to prevent a finger from growing further, we have to glue a cube to its boundary. Let us adopt the notation from [2] and denote the loop-correlation-function defined through sums over tree surfaces by $G_\beta^\infty(\gamma_1,\ldots,\gamma_n)$. Furthermore the subset of tree surfaces with boundary γ which cannot be divided into two pieces by cutting along a single link belonging to γ define the reduced loop-correlation-function $X_\beta(\gamma)$. By using arguments similar to those of Durhuus, Fröhlich and Jonsson [2], we obtain for large dimensions:

$$G_\beta^\infty(\gamma) = \frac{X_\beta(\gamma)}{1 - X_\beta(\gamma)} \tag{6.1}$$

and

$$X_\beta(\gamma) = 2d\,\mathrm{e}^{-2\beta}\big(G_\beta^\infty(\gamma)\big)^3 + (2d)^2\mathrm{e}^{-6\beta}\big(1 + G_\beta^\infty(\gamma)\big)^{11}. \tag{6.2}$$

Here γ stands for loops of length two. These equations only contain the leading terms for large d. The neglected terms yield subdominant contributions to the quantities considered in the following. If we define $u := 2d\,\mathrm{e}^{-2\beta}$ we obtain from (6.1) and (6.2)

$$u^3 + 2d(1-X)^8X^3u - 2d(1-X)^{11}X = 0, \tag{6.3}$$

where X is shorthand notation for $X_\beta(\gamma)$. At the critical point the derivative of X with respect to u has to be singular, which means

$$\left.\frac{\mathrm{d}u}{\mathrm{d}X}\right|_{X_\mathrm{c}} = 0, \tag{6.4}$$

with $X_\mathrm{c} := X_{\beta_0}(\gamma)$. Differentiating (6.3) with respect to X gives

$$u(X_\mathrm{c}) = \frac{(1-X_\mathrm{c})^3(1-12X_\mathrm{c})}{X_\mathrm{c}^2(3-11X_\mathrm{c})}. \tag{6.5}$$

Inserting this into (6.3) implies

$$2d = \frac{(1-12X_\mathrm{c})^3}{X_\mathrm{c}^7\big((3-11X_\mathrm{c})(1-X_\mathrm{c})\big)^2(2+X_\mathrm{c})}. \tag{6.6}$$

Consistency requires

$$0 < X_\mathrm{c} < \tfrac{1}{12}. \tag{6.7}$$

From (6.6) we can compute X_c numerically, which, via (6.5) and the definition of u determines β_0. Combining (6.7) and (6.6) we see that X_c goes to zero as d goes to infinity. In this case we can expand the r.h.s. of (6.6) and obtain

$$X_c = (18 \cdot 2d)^{-1/7}\left(1 + O(d^{-1/7})\right) \qquad \text{for } d \to \infty . \tag{6.8}$$

Therefore the critical coupling constant goes asymptotically to

$$\beta_0^{\text{asym}} = \tfrac{5}{14}\log 2d + \tfrac{1}{14}\log\tfrac{3^3}{2^2} \qquad \text{for } d \to \infty . \tag{6.9}$$

Let us investigate what happens if we take cubes cut along their edges as tree elements. That is we do not take into account the possibility of having doubly occupied plaquettes. In this case (6.1) is still correct, whereas in (6.2) we have to leave off the first term on the r.h.s. For the critical coupling constant we obtain

$$\beta_0^{\text{cube}} = \tfrac{1}{3}\log 2d + \tfrac{1}{6}\log\frac{12^{12}}{11^{11}} . \tag{6.10}$$

In table 4 the behaviour of β_0^{cube}, β_0^{asym} and the full mean-field result β_0^{MF}, computed from (6.5), (6.6) is compared for various dimensions. The interesting fact is, that for small and intermediate d the full expression is almost saturated by the contribution from the cubes. At $d = 10^8$ it happens for the first time, that β_0^{asym} is closer to β_0^{MF} than β_0^{cube}. Finally at about $d = 10^{30}$ β_0^{MF} and β_0^{asym} are in very good agreement, whereas β_0^{cube} is significantly smaller.
It is amusing to see, that in high dimensions

$$\beta_0^{\text{PRS}} = \tfrac{1}{2}\log 2d + c ,$$

$$\beta_0^{\text{cube}} = \tfrac{1}{3}\log 2d + c' ,$$

$$\beta_0^{\text{SARS}} = \tfrac{1}{4}\log 2d + c'' . \tag{6.11}$$

In fig. 2 the behaviour of β_0^{MF} and the measured values of β_0 is depicted. Below $d = 8$ the measured values are lower than β_0^{MF} ($\approx \beta_0^{\text{cube}}$), whereas above $d = 8$ the MC values show a trend to be slightly larger than β_0^{MF}. Nevertheless β_0^{MF} seems to be a fairly good approximation for β_0^{PRSWS} if one works in dimensions larger or equal to six.

Let us emphasize a difference in the large d behaviour of PRS and PRSWS. In PRS the value of X at the critical point is $\frac{1}{4}$. For the model without spikes X_c vanishes for d going to infinity, as has been noted before. Consider the string tension:

$$\tau(\beta) := -\lim_{L,M\to\infty} \frac{1}{LM}\log G_\beta(\gamma_{L,M}) , \tag{6.12}$$

TABLE 4
Comparison of different β_0 for various d

d	β_0^{MF}	β_0^{cube}	β_0^{asym}
3	1.1718	1.1709	0.7763
4	1.2678	1.2668	0.8791
5	1.3422	1.3412	0.9587
6	1.4031	1.4020	1.0239
7	1.4545	1.4534	1.0789
8	1.4991	1.4979	1.1266
9	1.5384	1.5371	1.1687
10	1.5735	1.5723	1.2063
12	1.6344	1.6330	1.2714
14	1.6858	1.6844	1.3265
16	1.7304	1.7289	1.3742
18	1.7697	1.7682	1.4162
20	1.8049	1.8033	1.4539
22	1.8367	1.8351	1.4879
24	1.8658	1.8641	1.5190
26	1.8925	1.8908	1.5476
10^2	2.3425	2.3398	2.0287
10^3	3.1129	3.1073	2.8510
10^4	3.8860	3.8748	3.6734
10^5	4.6635	4.6424	4.4957
10^6	5.4471	5.4099	5.3181
10^7	6.2376	6.1774	6.1404
10^8	7.0349	6.9450	6.9628
10^{10}	8.6461	8.4800	8.6075
10^{14}	11.9075	11.5501	11.8969
10^{20}	16.8325	16.1553	16.8310
10^{25}	20.9430	19.9929	20.9427
10^{30}	25.0546	23.8306	25.0545

where $\gamma_{L,M}$ is a rectangular loop of size LM. If the dominant contribution to $G_\beta(\gamma_{LM})$ comes from surfaces which are obtained by glueing trees to the minimal surface spanned by γ_{LM}, we have

$$\tau^\infty(\beta) = \beta + 2\log\bigl(1 - X_\beta(\gamma)\bigr). \tag{6.13}$$

Therefore in PRS

$$\tau^\infty_{\mathrm{PRS}}(\beta_0, d) = \beta_0^{\mathrm{PRS}}(d) + 2\log\tfrac{3}{4} \tag{6.14}$$

and in PRSWS for $d \to \infty$

$$\begin{aligned}\tau^\infty_{\mathrm{PRSW}}(\beta_0, d) &= \beta_0^{\mathrm{asym}}(d) + 2\log\bigl(1 - (18\cdot 2d)^{-1/7}\bigr)\\ &\to \beta_0^{\mathrm{asym}}(d).\end{aligned} \tag{6.15}$$

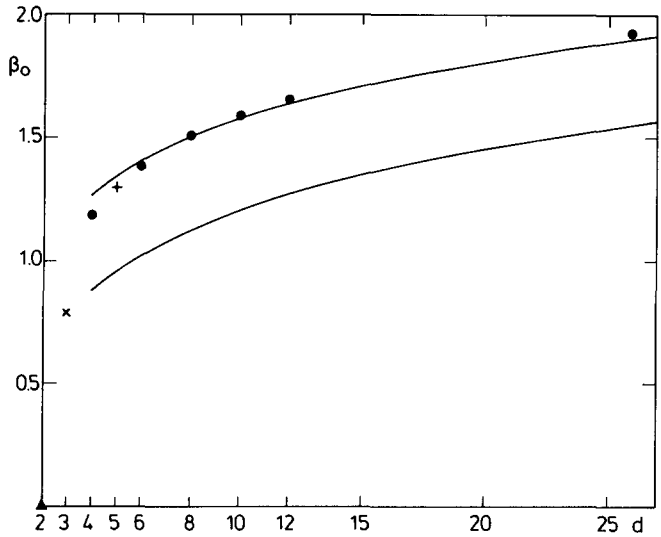

Fig. 2. The critical coupling constant versus the dimension of the embedding space. The dots represent the measured values obtained as explained in sect. 5. The error bars are smaller than the points. The upper curve portraits β_0^{MF} (or β_0^{cube}, which cannot be distinguished within the resolution of the drawing), the lower curve represents β_0^{asym}. In three dimensions only a part of the surface space is accessible (see ref. [7]). The value in 5 dimensions is taken from ref. [6]. In $d=2$ we define β_0 as the value of β, for which the string tension vanishes.

This means, that unlike the case of the PRS in infinite dimensions the string tension in PRSWS is dominated by the minimal surface alone–the trees are no more important! This shows that the PRSWS has features different from the PRS even in high dimensions.

I would like to thank Bernd Berg who initiated my interest in random surfaces and for discussions on the modified MC algorithm. I am indebted to Gernot Münster for continuous encouragement, in particular for keeping care that I did not get lost in high dimensions. Thanks are due to Peter Weisz for reading the manuscript. I am grateful to the "Rechenzentrum der Universität Hamburg" for generous support with computer time. Finally I would like to thank the "Supercomputer Computations Research Institute" at the Florida State University in Tallahassee, Florida, where part of this work has been done, for a travel grant.

References

[1] B. Durhuus, J. Fröhlich and T. Jonsson, Phys. Lett. 137B (1984) 93
[2] B. Durhuus, J. Fröhlich and T. Jonsson, Nucl. Phys. B240 [FS12] (1984) 453
[3] J. Fröhlich, The statistical mechanics of surfaces, Sitges (1984), Conference Proceedings, p. 31
[4] B. Berg and D. Förster, Phys. Lett. 106B (1981) 323

[5] A. Guha and L. Roberts, University of Rochester preprints UR 913-ER13065-413 (1985), UR 933-DOE/ER/13065-433 (1986)
[6] B. Berg and A. Billoire, Phys. Lett. 139B (1984) 297
[7] B. Berg, A. Billoire and D. Förster, Nucl. Phys. B251 [FS13] (1985) 665
[8] A. Berretti and A. D. Sokal, J. Stat. Phys. 40 (1985) 483
[9] Ph. de Forcrand, F. Koukiou and D. Petritis, Univ. de Lausanne preprint (1985)
[10] B. Baumann and B. Berg, Phys. Lett. 164B (1985) 131
[11] T. Jonsson, Comm. Math. Phys. 106 (1986) 679
[12] G. Münster, private communication
[13] J.M. Drouffe, G. Parisi and N. Sourlas, Nucl. Phys. B161 (1980) 397
[14] B. Durhuus, J. Fröhlich and T. Jonsson, Nucl. Phys. B225 [FS9] (1983) 185
[15] B. Durhuus, J. Fröhlich and T. Jonsson, Nucl. Phys. B257 [FS14] (1985) 779
[16] D.B. Abraham, J.T. Chayes and L. Chayes, Phys. Rev. D30 (1984) 841; Comm. Math. Phys. 96 (1984) 439; Nucl. Phys. B251 [FS13] (1985) 553
[17] B. Durhuus and T. Jonsson, University of Iceland preprint RH-04-86 (1986)
[18] A. Polyakov, Nucl. Phys. B268 [FS14] (1986) 406